

Water Resources Research

RESEARCH ARTICLE

10.1002/2015WR017395

Key Points:

- Infiltration and recharge zones on the beachface varied temporally and spatially
- Steady unsaturated recharge to the aquifer occurred at swash and tidal time scales
- Subsurface observations are needed to delineate infiltration and discharge zones

Correspondence to:

H. A. Michael,
hmichael@udel.edu

Citation:

Heiss, J. W., J. A. Puleo, W. J. Ullman, and H. A. Michael (2015), Coupled surface-subsurface hydrologic measurements reveal infiltration, recharge, and discharge dynamics across the swash zone of a sandy beach, *Water Resour. Res.*, 51, doi:10.1002/2015WR017395.

Received 13 APR 2015

Accepted 10 OCT 2015

Accepted article online 15 OCT 2015

Coupled surface-subsurface hydrologic measurements reveal infiltration, recharge, and discharge dynamics across the swash zone of a sandy beach

James W. Heiss¹, Jack A. Puleo², William J. Ullman^{1,3}, and Holly A. Michael^{1,2}

¹Department of Geological Sciences, University of Delaware, Newark, Delaware, USA, ²Department of Civil and Environmental Engineering, University of Delaware, Newark, Delaware, USA, ³School of Marine Science and Policy, University of Delaware, Lewes, Delaware, USA

Abstract Swash-groundwater interactions affect the biogeochemistry of beach aquifers and the transport of solutes and sediment across the beachface. Improved understanding of the complex, coupled dynamics of surface and subsurface flow processes in the swash zone is required to better estimate chemical fluxes to the sea and predict the morphological evolution of beaches. Simultaneous high-frequency measurements of saturation, water table elevation, and the cross-shore locations of runup and the boundary between the saturated and unsaturated beachface (surface saturation boundary) were collected on a sandy beach to link groundwater flow dynamics with swash zone forcing. Saturation and lysimeter measurements showed the dynamic response of subsurface saturation to swash events and permitted estimation of infiltration rates. Surface and subsurface observations revealed a decoupling of the surface saturation boundary and the intersection between the water table and the beachface. Surface measurements alone were insufficient to delineate the infiltration and discharge zones, which moved independently of the surface saturation boundary. Results show for the first time the motion and areal extent of infiltration and recharge zones, and constrain the maximum size of the subaerial discharge zone over swash and tidal time scales. The width of the infiltration zone was controlled by swash processes, and subaerial discharge was controlled primarily by tidal processes. These dynamics reveal the tightly coupled nature of surface and subsurface processes over multiple time scales, with implications for sediment transport and fluid and solute fluxes through the hydrologically and biogeochemically active intertidal zone of sandy beaches.

1. Introduction

Groundwater-surface water interactions in the intertidal zone are recognized as an important factor in beach biogeochemistry and morphology. Fluid exchange across the aquifer-ocean interface can lead to mixing between seawater and discharging fresh groundwater in coastal aquifers. Mixing can alter the biogeochemistry of sandy beach aquifers [e.g., Charette and Sholkovitz, 2002; Kroeger and Charette, 2008; Spiteri et al., 2008; Santoro, 2010; Anwar et al., 2014; McAllister et al., 2015] and influence solute concentrations in groundwater prior to discharge [Santos et al., 2008; Roy et al., 2010; Sawyer et al., 2014]. Seawater can also introduce organic matter and dissolved oxygen to shallow beach sediments, driving aerobic and anaerobic respiration [McLachlan et al., 1985; Ullman et al., 2003; Orr et al., 2005; Charbonnier et al., 2013].

Groundwater-surface water exchange also affects sediment transport processes by altering the thickness of the boundary layer and the effective weight of the sediment [Nielsen, 1992]. Infiltration during runup increases bed shear stress due to a thinning of the boundary layer, which promotes onshore sediment transport while simultaneously increasing the effective weight of immersed sediment, which decreases the potential for onshore sediment transport. The opposite occurs during rundown when discharge thickens the boundary layer and reduces shear stress. This decreases the potential for offshore transport, but effective sediment weight is simultaneously reduced due to discharge, promoting offshore sediment transport. The effects of infiltration and discharge on the relative importance of effective sediment weight versus boundary layer effects have been numerically [e.g., Masselink and Li, 2001; Karambas, 2003; Hoque and Asano, 2007; Bakhtyar et al., 2011] and experimentally [Turner and Masselink, 1998; Butt et al., 2001] investigated. Effective sediment weight dominates and offshore transport is promoted for grain sizes below

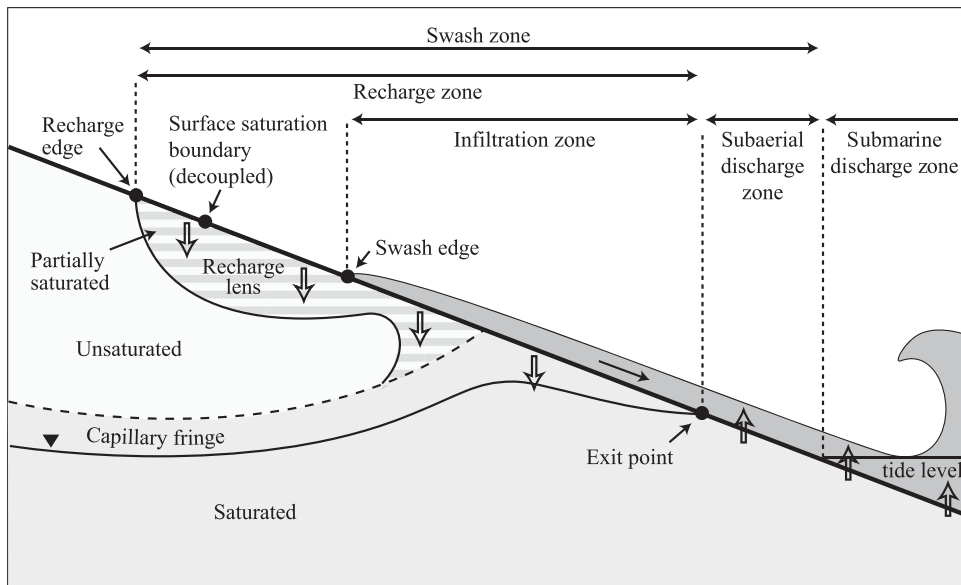


Figure 1. Schematic of surface water and groundwater levels in the swash zone. The locations of the infiltration, recharge, and discharge zones move across the beachface with the tide.

0.4–0.6 mm. For larger grain sizes, the effects of a modified boundary layer dominate and net transport is onshore [Karambas, 2003; Butt et al., 2001].

The swash zone, the area between the locations of maximum wave rundown and runup, is a dynamic area of groundwater-surface water exchange and is thus important to the biological, biogeochemical, and morphological evolution of beaches. Within the swash zone, the location of the intersection of the water table and beach surface has been termed the exit point [Turner, 1993], because it can mark a divide between zones of infiltration and discharge (Figure 1). Where that is the case, vertical infiltration occurs landward of the exit point across an intermittently saturated beachface, while subaerial groundwater discharge occurs seaward of the exit point across the permanently saturated lower beachface (Figure 1). Farther seaward, submarine groundwater discharge occurs below the tide level (Figure 1). Pore pressure response to swash motion below the infiltration and discharge zones has been investigated in a number of field and modeling studies [e.g., Waddell, 1976; Packwood and Peregrine, 1980; Hegge and Masselink, 1991; Turner and Nielsen, 1997; Horn et al., 1998; Turner and Masselink, 1998; Baldock et al., 2001; Butt et al., 2001]. These studies demonstrated that pore pressure response generally decreases with distance landward and depth below the sand surface. The resulting hydraulic gradients drive vertical flow across the beachface. Field, laboratory, and numerical modeling investigations have shown that vertical flow landward of the exit point within the swash zone is spatially and temporally variable [McLachlan et al., 1985; Kang et al., 1994; Steenhauer et al., 2011, 2012; Masselink and Turner, 2012; Heiss et al., 2014; Geng and Boufadel, 2015]. Infiltration within this zone affects saturation as water flows downward to the water table [Steenhauer et al., 2011, 2012; Geng and Boufadel, 2015] and may contribute significantly to total flow through the beach aquifer [McLachlan et al., 1985; Heiss et al., 2014]. Groundwater discharge in the intertidal zone seaward of the exit point also varies over time and space [Turner and Masselink, 1998; Li et al., 1999; Butt et al., 2001; Hays and Ullman, 2007; Michael et al., 2011; Rosenberry et al., 2013]. The location of the exit point has been identified in prior work as the interface between the unsaturated and saturated beachface (hereafter referred to as the *surface saturation boundary*), the area seaward of which appears as a shiny and glassy surface [Aagaard and Holm, 1989; Holman et al., 1993; Cartwright et al., 2006; Puleo, 2009; Huisman et al., 2011; Voudoukas, 2014].

The dynamics of the surface saturation boundary have been the focus of previous field studies investigating groundwater-surface water interactions in the swash zone. Red-green-blue (RGB) imaging systems have been used to identify and track the surface saturation boundary as a proxy for subaerial discharge at the time scale of individual swash events, as this technique provides continuous data collection at high spatial and temporal resolution [Aagaard and Holm, 1989; Holman et al., 1993; Puleo, 2009; Huisman et al., 2011; Voudoukas, 2014]. The surface saturation boundary can also be tracked manually by visual inspection of

the beachface [Cartwright *et al.*, 2006]. The subaerial discharge zone can be monitored directly from water table measurements using a cross-shore transect of monitoring wells [Turner, 1993; Turner and Masselink, 1998; Huisman *et al.*, 2011]. Huisman *et al.* [2011] combined observations of the surface saturation boundary with water table measurements and demonstrated that the surface saturation boundary corresponded to the location on the beachface where the water table was within 2 cm of the surface. In that study, the surface saturation boundary was coincident with the exit point, was landward of the swash zone, and displayed low-frequency motion related to tidal phase. Others have shown that the surface saturation boundary moves across the beach in response to individual swash events [e.g., Cartwright *et al.*, 2006; Puleo, 2009; Voudoukas, 2014]. However, the extent to which the location and motion of the surface saturation boundary at the swash time scale is representative of the location and dynamics of the water table-beachface intersection remains unclear. Combined surface and subsurface observations at high temporal and spatial resolution are needed to investigate the extent of this coupling and to identify and the boundary between zones of groundwater-surface water exchange

In addition to the need to better link surface conditions to infiltration and discharge zones, there is a need to connect surface conditions to flow in the unsaturated zone. Coupling between swash and groundwater flow in the saturated zone has been investigated extensively. Pore pressure fluctuations in the saturated beach in response to runup have been tied to surface dynamics such as the location of the leading edge of the swash lens (hereafter referred to as the swash edge) [Hegge and Masselink, 1991], swash velocity [Butt *et al.*, 2001] and depth [Turner and Masselink, 1998], the location across the swash zone [Austin and Masselink, 2006], surf zone conditions [Sous *et al.*, 2013], and proximity to the surface saturation boundary [Cartwright *et al.*, 2006]. However, fewer field studies have instrumented the unsaturated zone to monitor unsaturated groundwater flow in response to swash processes [e.g., Horn *et al.*, 1998; Baldock *et al.*, 2001; Heiss *et al.*, 2014]. Although these three field studies offer valuable insight into unsaturated flow processes, the measurements were limited to the subsurface. Pore pressure [e.g., Horn *et al.*, 1998] and subsurface water content [e.g., Heiss *et al.*, 2014] measurements collected within the unsaturated zone have revealed a region of nearly saturated sediment immediately below the sand surface that forms as a result of swash inundation and infiltration across the unsaturated beachface. A zone of unsaturated sediment divides the recharge lens from the water table at depth (Figure 1) [Horn *et al.*, 1998; Heiss *et al.*, 2014] until saturation occurs due to a combination of the downward movement of the recharge lens and a rising water table and capillary fringe from below [Heiss *et al.*, 2014]. Steenhauer *et al.* [2011] conducted laboratory experiments to couple the swash edge location with unsaturated flow. They used digital imaging techniques and pore pressure measurements in a series of carefully controlled tests in cemented and immobile sediment to demonstrate important linkages between the location of the swash edge and the dynamics of the recharge lens including its shape, horizontal and vertical extent, volume, and downward velocity following a dam-break-driven swash event. The results revealed decoupling between swash and unsaturated flow where the recharge lens continued to move downward through unsaturated sediment to the water table following rundown. Most infiltrating water in the laboratory beach with 1.5 mm diameter sediment remained in the shallow unsaturated zone and moved downward slowly. In sediment of 8.5 mm diameter, the recharge lens was thicker and moved downward more rapidly. The water table-beachface intersection was also decoupled from the swash edge in both beaches. The findings demonstrate that infiltration into and flow though the unsaturated zone should be considered when evaluating subsurface flow behavior. Austin and Masselink [2006] used pore pressure measurements below the water table in the swash zone and observed similar decoupling behavior in a steep gravel beach. The saturated pore pressure measurements were used to infer a downward motion of the recharge lens to the water table. However, the structure and dynamics of the recharge lens and flow through the unsaturated zone were not directly examined. As a result, it remains unclear how the swash edge, surface saturation boundary, and exit point are coupled to pore water flow through the unsaturated zone over multiple swash events and over a tidal cycle in a natural beach setting.

We expand on previous studies by simultaneously measuring surface and subsurface processes to investigate the coupling between the swash edge and surface saturation boundary, and the groundwater dynamics in the saturated and unsaturated zones of a sandy beach aquifer. The objectives of this work are to (1) investigate the dynamics of infiltration and discharge zones as they relate to the location of the swash edge, surface saturation boundary, and tide level, (2) link saturated and unsaturated flow processes with

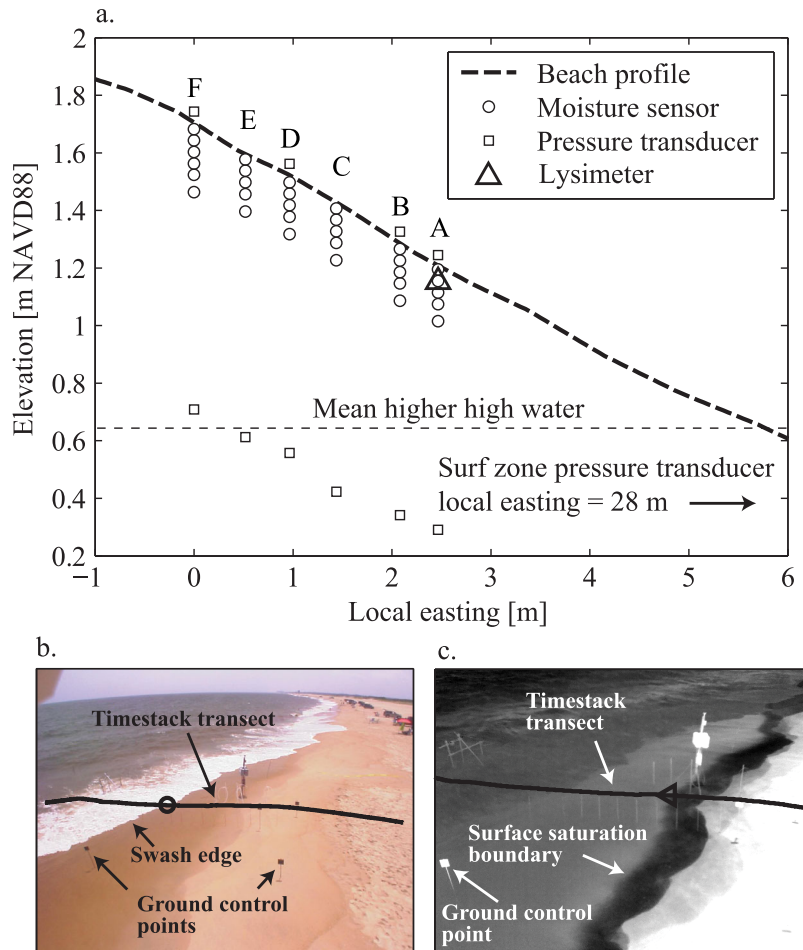


Figure 2. Instrument deployment for the field study. (a) Sensor transect and beach profile. Labels A–F indicate vertical array site location. The triangle is the position of the lysimeter separated 0.5 m in the alongshore direction from the main cross-shore instrument transect. (b) View from RGB imager showing swash edge (circle). (c) View from thermal imager showing surface saturation boundary (triangle). The black curves in Figures 2b and 2c are the pixel coordinates of the timestack transect.

swash and tidal forcing, and (3) provide new insight into groundwater-surface water interactions within the swash zone.

2. Field Experiment

2.1. Study Site

A field experiment was conducted on 27 June, 2013 at Herring Point, Cape Henlopen, Delaware ($38^{\circ}45'51.8''N$, $75^{\circ}04'54.0''W$) on the U.S. mid-Atlantic seaboard. Cape Henlopen is a sandy spit where long-shore currents transport sediment northward along its Atlantic boundary. The morphology of the beach consists of a dune, a flat backshore, and a 30 m wide beachface with a 1:6 slope. Grain size analysis of sediment collected from the site indicates that the intertidal zone is comprised of medium sand with a median grain size of 0.39 mm. Constant head permeameter tests yielded a hydraulic conductivity of 21 m d^{-1} . Off-shore significant wave height and period recorded 47 km to the southeast by the National Data Buoy Center Station 44009 during the experiment were 0.89 m and 8.7 s, respectively. Tides are semidiurnal with a mean range of 1.4 m (NOAA tidal station 8557830, Lewes, Delaware).

2.2. Instrumentation

Volumetric water content and water table elevation were monitored using a cross-shore transect of moisture sensors and pressure transducers (Figure 2). The transect was deployed in the section of the beach that extended from 3.5 to 6.0 m landward of the high tide mark and included six instrument arrays separated

horizontally by approximately 0.5 m. Each array, labeled Sites A through F in Figure 2, was outfitted with 5–6 moisture sensors (Decagon Devices EC-5) to measure volumetric water content at various depths in the unsaturated zone. Moisture sensors were pushed horizontally into the undisturbed sediment along the wall of an augured hole in an effort to measure water content at the natural bulk density of the beach. Volumetric water content was converted to local saturation at all moisture sensor locations using the porosity measured by each sensor. The sensors were installed in vertical arrays at depths of 2, 6, 10, 14, and 18 cm below the beach surface. An additional moisture sensor was installed at a depth of 24 cm at Site F. All arrays were equipped with a pressure transducer (Druck PTX 1835 or Druck PTX 1830) placed in the saturated zone to measure the water table, and four arrays had a second pressure transducer positioned at the sand surface to measure swash depth. A manometer with two 1 cm screens separated vertically by 40 cm was used to observe vertical head differences in the saturated beach below the swash zone in order to ensure that vertical gradients were low enough that pore pressure measurements could be used to estimate the water table height. The head difference was consistently ≤ 1.5 mm, which is within the measurement error of the pressure transducers and 3% of head fluctuations, which were typically 5 cm. A pressure transducer was positioned in the inner surf zone to measure local incoming wave height and period. Cables were routed away from the transect and buried in a trench leading up the beach. Water content and pressure were recorded at 5 and 16 Hz, respectively.

The slope of the measured water table between the two most seaward pressure transducers was linearly extrapolated to the sand surface [e.g., *Turner*, 1993; *Turner and Masselink*, 1998; *Huisman et al.*, 2011]. The point of contact between the extrapolated water table and beachface is referred to as the extrapolated water table-beachface intersection. The distinction between the extrapolated water table-beachface intersection and the exit point is discussed in section 3.1.1.

The motion of the swash edge and surface saturation boundary were tracked using two different imagers. A Sony DFW-X710 RGB imager (1024×768 pixels) recorded visible-band imagery at 4 Hz to identify the swash edge. The image sequence was recorded as individual time-stamped frames as joint picture experiment group (.jpeg) images. Thermal infrared imagery was captured using a FLIR systems SC645 imager (640×480 pixels) recording at 3.125 Hz to identify the surface saturation boundary. Thermal imagery was recorded using FLIR software in their proprietary format and later converted to a windows media file (.wmv) for analysis. The main focus for thermal imagery was the contrast between the saturated and unsaturated beachface. Therefore, the actual kinetic temperature was not calculated. Parameters such as emissivity in the internal conversion from radiance to temperature were chosen based on water (0.98) and local conditions. Contrast was enhanced by altering the temperature scale versus image intensity within the image sequence prior to file conversion. The uncertainty in the location of the surface saturation boundary is estimated to be ± 12 cm. This was calculated based on the slope of the beach (1:6) and the depth of the shallowest moisture sensors (2 cm), above which saturation could not be directly measured to confirm the imagery. This uncertainty is $\sim 1\%$ of the width of the swash zone during the experiment. Images were recorded in Coordinated Universal Time (UTC) and converted to local time where the beginning of the run is relative to 13:33:00 UTC.

The imagers were mounted on top of a 6 m aluminum tower in the back beach 20 m orthogonal (in the alongshore) to the transect such that the field of view was oblique relative to the study area (Figures 2b and 2c). The locations of the swash edge and surface saturation boundary were extracted from time stack images collected near the instrument transect. A time stack is a cross-shore transect of pixel intensity from each sequential frame in the image sequence [*Aagaard and Holm*, 1989; *Holman et al.*, 1993; *Holland and Holman*, 1993]. The pixel coordinates of the cross-shore transect (Figures 2b and 2c; black curves) were identified in the image using a geometrical model (including lens distortion) based on the camera position and surveyed ground control points (rectangular targets in Figures 2b and 2c) within the image [*Holland et al.*, 1997]. The model allows for conversion from real world to pixel coordinates using the measured beach profile. The swash edge is clearly identifiable in the visible band [*Aagaard and Holm*, 1989; *Holman et al.*, 1993; *Puleo*, 2009] while the surface saturation boundary is most pronounced in thermal images as a result of the temperature contrast between the dry and wet beach surface. An edge-detection algorithm based on pixel intensity differences was used to automatically detect the location of the two boundaries and hence the time history of the saturation and swash edge location. The algorithm is imperfect and requires manual correction where it clearly does not track the feature of interest. The amount of manual

correction was estimated as 10% of the time series. A real time kinematic global position system (RTK-GPS) survey was performed on the day of the experiment quantifying the sensor positions, the local beach topography and the ground control points needed for geometrical transformation of images. Positions were collected in Universal Transverse Mercator (UTM) using North American Datum (NAD83) in the horizontal and North American Vertical Datum (NAVD88) in the vertical. Mean sea level in the area is roughly -0.1 m NAVD88. UTM coordinates were converted to a local northing-easting coordinate system with the origin at Site F to simplify understanding of distances on presented figures.

The experiment began midway through rising tide, continued into high tide, and concluded midway into the following ebb tide for a total of 8.5 h of data collection. Local significant wave height (0.57 m) was estimated as 4 times the standard deviation of the free-surface elevation time series from the inner surf-zone pressure transducer after removing the tidal signal. The local mean period (5.2 s) was determined using the zero up-crossing method on the free-surface time series. Saturation and pressure were recorded to three data loggers (National Instruments and Campbell Scientific) and imagery was recorded to two laptop computers. All devices were time synchronized using a Garmin GPS antenna, and Tac32 and Dimension4 software.

Swash infiltration across the saturated beach landward of the extrapolated water table-beachface intersection was measured using a pan lysimeter [Jordan, 1968]. The lysimeter consisted of a cylinder constructed from 10 cm ID polyvinyl chloride (PVC) pipe with a length of 20 cm [see Thompson and Scharf, 1994]. The bottom of the cylinder was sealed and the top was outfitted with a porous plate and mesh. A stand-alone pressure sensor placed in the lysimeter measured water depth at 2 Hz. Atmospheric pressure was maintained inside the device by venting the buried container to the sand surface with polyethylene tubing, providing an outlet for air as water flowed into the lysimeter. A perched water table must form along the top of the device in order for water to infiltrate [Jemison and Fox, 1992; Zhu et al., 2002]. Conventionally, pan lysimeters are buried in the unsaturated zone in agricultural and forested settings where pressure head is negative relative to the atmospheric pressure in the container. Consequently, soil suction can cause a considerable portion of flow to diverge around lysimeters yielding collection efficiencies that typically range between 10 and 60% of the total percolate [Russell and Ewel, 1985; Jemison and Fox, 1992; Zhu et al., 2002], with higher collection efficiencies under wet conditions and large vertical flow rates [Peters and Durner, 2009]. Initial laboratory and field tests at the study site indicated that the lysimeter collected infiltrating water across the lower saturated swash zone when the capillary fringe was at the sand surface, resulting in apparent collection efficiencies greater than 350%. A 2.5 cm divergence control tube [e.g., Bews et al., 1997] was added to the top of the lysimeter to calibrate the device to a collection efficiency near 100%. The control tube was filled with sand finer than the ambient sediment to impede flow into the device and to promote formation of a perched water table. A bench-top test was performed for the lysimeter in a chamber filled with sediment from the study site. Water was added to the sand surface at various periods (5–100 s) and to a range of depths (1–35 cm) to simulate swash inundation. Collection efficiencies ranged from 95 to 116%. Efficiencies greater than 100% were found when the period between inundation events was 5–25 s and inundation depths were 10–35 cm. Efficiencies from 95 to 100% occurred for inundation events with longer periods (25–100 s) and shallower depths (1–7 cm), the typical range for swash during the experiment. The pan lysimeter was installed 6 cm below the sand surface at Site A to test its utility for measuring saturated swash infiltration across the seaward swash zone and to compare saturated infiltration rates to unsaturated infiltration rates farther landward.

Swash-driven infiltration across the unsaturated beachface was calculated using saturation profiles from the vertical arrays of moisture sensors (see Heiss et al. [2014] for a more detailed description of the methodology). The technique is similar to the numerical scheme developed by Talbot and Ogden [2008] where infiltration is estimated as the difference between subsurface saturation before and after an infiltration event. Saturation at the shallowest sensor was the first to increase following swash inundation of the beachface at each site. It was assumed that once saturation at the shallowest sensor peaked, the volume of infiltrating water was enclosed within the region extending from the sand surface to 10 cm. This was based on the observation that saturation at the shallowest sensor began to decline before rising at the third deepest sensor at 10 cm depth (saturation at sensors below this depth remained constant for the swash events considered). The volume of water that infiltrated the beach due to individual swash events at each site was calculated as the difference in the saturation, accounting for porosity, along the vertical profile immediately prior to swash inundation (T_1) and at the

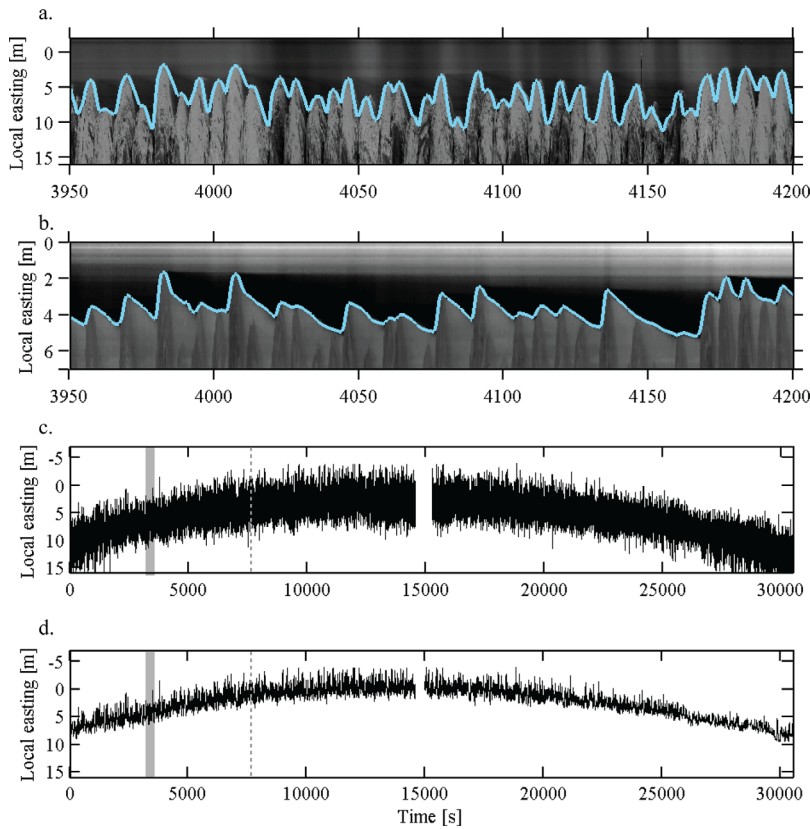


Figure 3. Swash zone runup and surface saturation boundaries. (a) Example visible-band RGB time stack imagery for a period of 250 s, showing detected swash edge in blue. The gray scale is pixel intensity; (b) example thermal time stack imagery showing surface saturation boundary in blue for the same period as Figure 3a. The gray scale is temperature mapped to pixel intensity; entire (c) runup and (d) surface saturation boundary time series extracted from the timestacks. The gray shading in Figures 3c and 3d shows the time range presented in Figures 3a and 3b. The dotted vertical gray line in Figures 3c and 3d shows the time presented in Figure 4. Local easting is meters relative to the farthest landward site (Site F). Negative easting is landward and positive easting is seaward.

time that the shallowest sensor signal peaked (T_2). By fitting a line to the vertical profile at time T_1 and an exponential function at time T_2 , unsaturated swash infiltration per swash event D_{su} is:

$$D_{su} = \int_{-Z_{MS3}}^0 \eta S_{T2}(z) dz - \int_{-Z_{MS3}}^0 \eta S_{T1}(z) dz \quad (1)$$

where $S_{T2}(z)$ is the saturation S as a function of depth z at T_2 , $S_{T1}(z)$ is the saturation as a function of depth at T_1 , η is porosity, and Z_{MS3} is the depth of the third moisture sensor from the surface.

Infiltration for six closely spaced swash events was calculated using equation (1) and the results were paired with the lysimeter values for the same set of swash events to develop an infiltration profile from the seaward saturated swash zone to the landward unsaturated swash zone.

3. Results

The imagers captured the location of the swash edge and surface saturation boundary. The swash edge is identifiable in the visible-band time stack by the bright rapidly moving feature across the beachface (Figure 3a). The surface saturation boundary is shown in the thermal imagery as the bright, more slowly seaward moving feature (Figure 3b). The effect of the tide on the location of the swash edge and surface saturation boundary is evident from the curvature of the time series over the duration of the experiment (Figures 3c and 3d). The transect was landward of the runup limit from the start of the experiment to 5000 s and was periodically inundated by swash events from 5000 to 22,500 s (Figure 3c). The surface saturation boundary also passed over the transect from 5000 to 22,500 s, indicating that the instruments were located in the landward portion of the swash zone (Figure 3d).

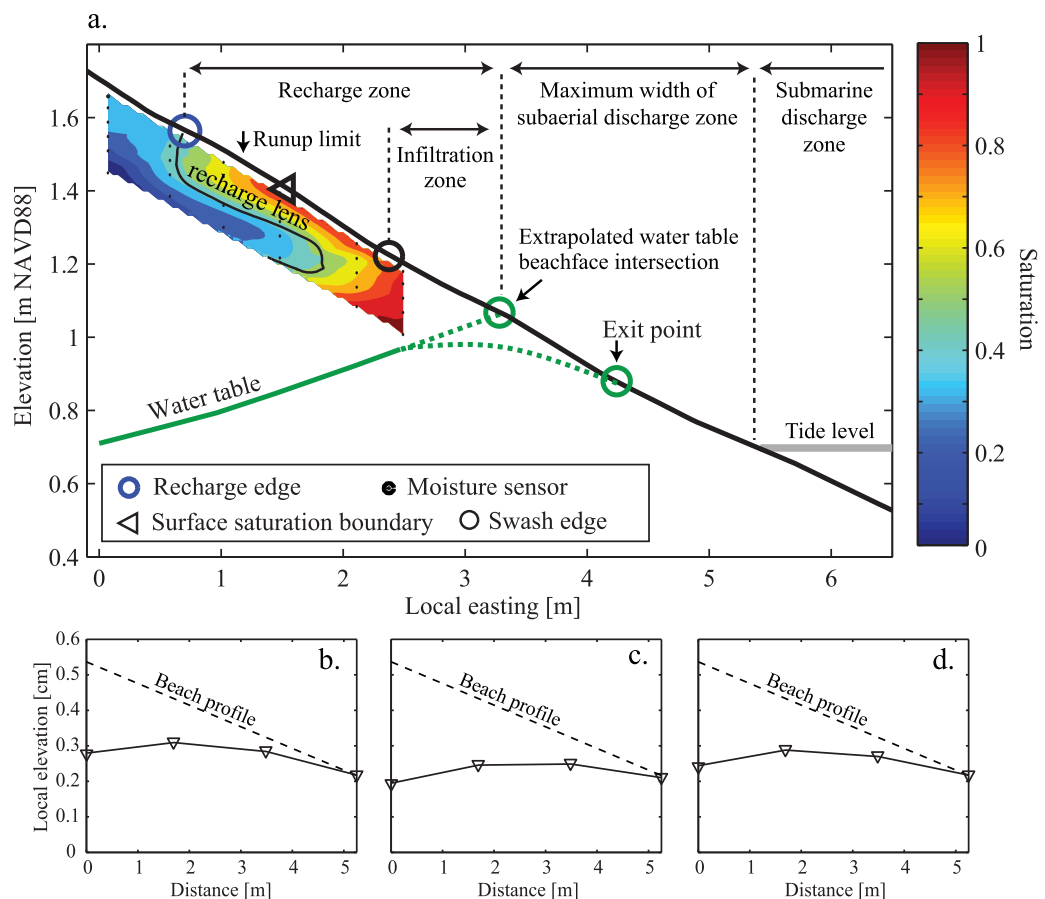


Figure 4. Instantaneous surface and subsurface conditions during rising tide at 7640 s (see Figures 3c and 3d). (a) Subsurface saturation, water table, surface features, and surface zonation. Zero indicates fully unsaturated conditions and 1 indicates fully saturated conditions. The black contour is the boundary of the recharge lens. Dashed green lines indicate potential water table configurations seaward of measurements. Measured water table mound at (b) low, (c) mid, and (d) high tide marks from Heiss et al. [2014].

3.1. Saturation Beneath the Swash Zone

3.1.1. Identification of Surface and Subsurface Features

The surface and subsurface features shown in Figure 1 were identified from the field measurements. The instantaneous data from 7650 s (Figure 4) are used to illustrate these features. Swash infiltration occurred across the sand surface in the *infiltration zone*, defined as the area between the extrapolated water table-beachface intersection and the instantaneous location of the overriding swash edge (Figure 4). In effect, the infiltration zone was located landward of the extrapolated water table-beachface intersection where the beachface was currently inundated by swash. Saturation increased and then decreased in the unsaturated zone after the swash edge receded, hence there was downward vertical flow during times when the swash edge was seaward of the transect. This indicates that recharge was occurring where instantaneous infiltration was not. The region of vertical unsaturated flow is the *recharge lens* (see black contour in Figure 4), defined as the aquifer region where saturation was changing beneath the swash zone. The area of the beachface directly above the recharge lens and including the infiltration zone is the *recharge zone*. The *recharge edge* marks the landward extent of the recharge zone on the beachface.

The vertical flow direction across the sand surface seaward of the extrapolated water table-beachface intersection is unclear due to a lack of measurements in that zone and the resulting uncertainty in the slope of the water table in that section of the beach. When a water table mound exists due to swash infiltration, the seaward swash zone is characterized by a subaerial discharge zone with an exit point seaward of the extrapolated water table and extending to the cross-shore location of the tide level (Figure 4a). Conversely, the same region of the beachface can be characterized as a zone of subaerial recharge if the water table slopes landward. In this work, it is assumed that a water table mound and

exit point were present seaward of the transect based on previously reported observations from a variety of natural and laboratory beaches [e.g., Kang *et al.*, 1994; Boufadel *et al.*, 2007; Steenhauer *et al.*, 2011; Masselink and Turner, 2012; Turner and Masselink, 2012] and at this field site [Heiss *et al.*, 2014]. Heiss *et al.* [2014] monitored the water table elevation farther seaward in the swash zone and observed mounding near the low, mid, and high tide marks (Figures 4b–4d). Thus, the prior data support the existence of a water table mound and exit point on the rising tide, and because it is more likely that a mound exists on a falling tide, it is assumed that they exist throughout the tidal cycle at this site. A *subaerial discharge zone* exists between the exit point and the tide level (Figure 1). The location of the exit point could only be quantified near high tide because the exit point was located seaward of the measurement transect for the rest of the monitoring period. The extrapolated water table-beachface intersection is used to constrain the location of the exit point when the exit point is seaward of the transect. It is tracked as the farthest possible landward location of the exit point and constrains the maximum width of the subaerial discharge zone (Figure 4a). Additional discharge seaward of the tide level likely occurs in the *submarine discharge zone*.

The recharge lens and its origin due to infiltration were previously discussed in Heiss *et al.* [2014]. In the next three sections, those findings are extended by describing the structure of the recharge lens and saturation dynamics as they relate to the swash edge, the surface saturation boundary, and the tide levels over swash event and tidal time scales. The dynamics of the infiltration, recharge, and discharge zones are discussed in section 3.3.

3.1.2. Saturation Dynamics at the Swash Time Scale

Subsurface saturation was less dynamic than the swash edge. Figure 5a illustrates the conditions immediately prior to a swash event that inundated the sand surface within the full transect. Swash inundation that occurred prior to the time in Figure 5a produced a recharge lens in the upper 10 cm of sediment that extended landward to $x = 1.1$ m. The recharge edge moved landward roughly 0.5 m as the swash edge overrode Site F at 25 s (Figures 5b and 5h). Approximately 3 s later the recharge edge shifted beyond the landward limit of the transect (Figures 5c and 5h), and therefore could not be mapped in Figure 5h. Saturation increased marginally from 2 to 6 cm depth between Sites D and F in the time period between the initial subsurface conditions and the arrival of the second large swash event at 45 s (Figures 5c and 5d). It was not until after this second swash event at 45 s (Figure 5e) that saturation in the landward half of the unsaturated zone increased substantially due to infiltration (Figures 5d and 5e). Saturation in the shallow sediment at Site F then decreased and the recharge edge moved seaward back within the transect (Figure 5f). The damped movement of the recharge edge compared to the swash edge indicates that downward flow in the unsaturated zone and recharge to the aquifer continues after the swash recedes.

The movement of the lateral boundary between saturated and unsaturated sediments in the subsurface over swash events was muted compared to that at the surface (Figure 6). The subsurface saturation boundaries were defined by moisture measurements greater than 95% of saturation at that location, due to uncertainty in porosity and precision of the measurements. The surface saturation boundary moved up the beach 3.3 m in response to the swash event at 18 s while the subsurface saturation boundary at 2 cm depth moved 0.51 m. The dampening effect was more pronounced deeper in the unsaturated zone where the subsurface saturation boundary moved 0.38 m at 6 cm depth and 0.07 m at 10 cm depth (Figure 6). Analysis of the movement of the subsurface saturation boundary relative to that of the surface saturation boundary for five swash events indicates an exponential decay in the magnitude of fluctuation with depth (Figure 7a). The difference in the magnitude of the fluctuations demonstrates that infiltrating water entered the shallow unsaturated zone rapidly before draining more slowly downward at depth. The rapid and pulsed vertical infiltration resulted in large fluctuations in downward flow near the surface while more steady downward flow deeper in the unsaturated zone resulted in smaller changes in subsurface saturation.

In addition to dampening, there was a time lag between the movement of the surface saturation boundary and the subsurface saturation response over individual swashes. The time lag was calculated as the elapsed time between the arrival of the landward limit of the surface saturation boundary and the landward limit of the subsurface saturation boundary at a particular depth. The time lag between the surface and subsurface

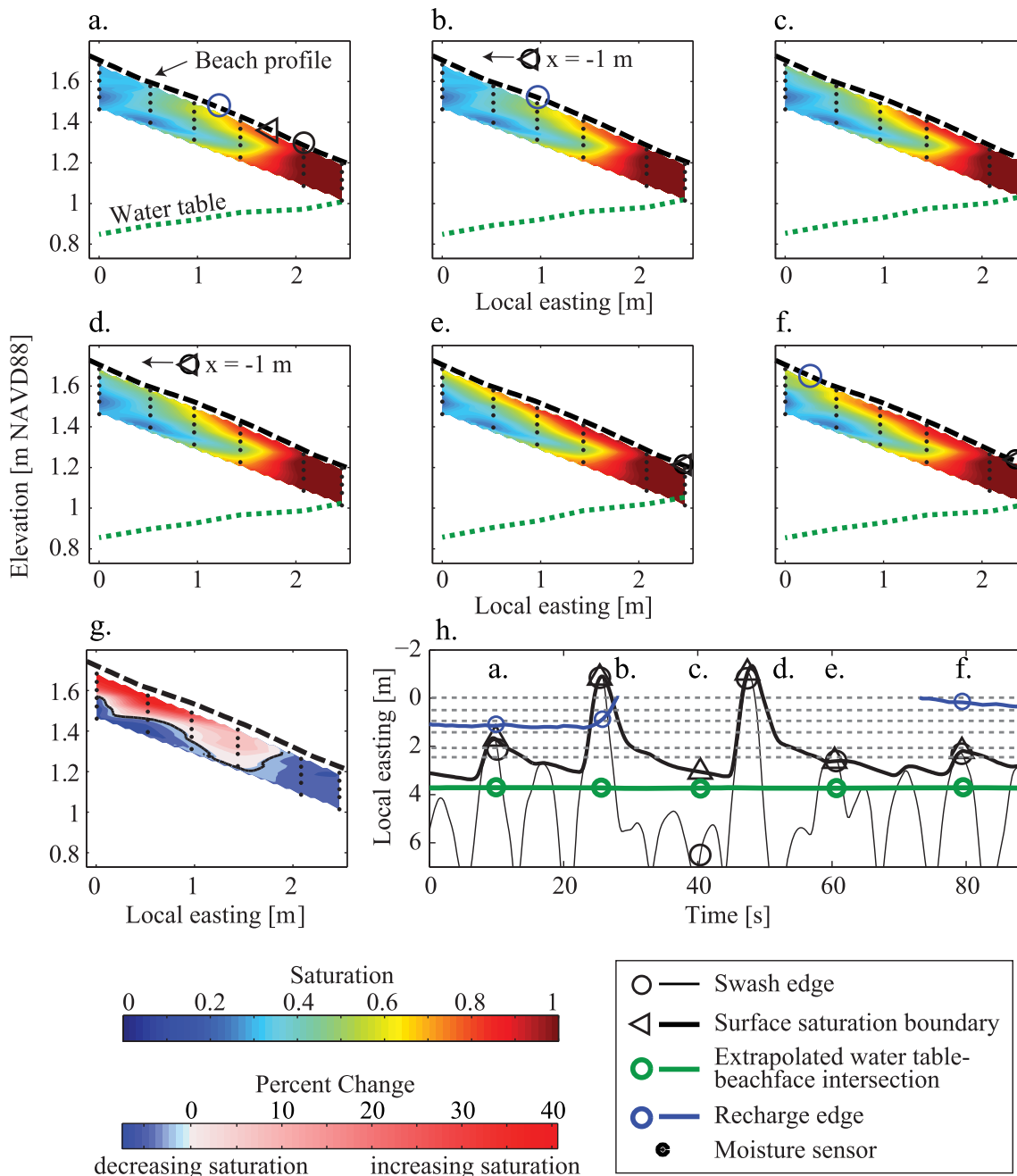


Figure 5. Subsurface saturation and surface features through two swash events that inundated the instrument transects between 8970 and 9039 s. (a–f) Subsurface saturation and water table before, during, and immediately following two swash events that inundated the full extent of the instrument transect. (g) Percent change in saturation between Figures 5a and 5f. Dashed horizontal lines in Figure 5h are the cross-shore positions of the instrument sites. The positions of the swash edge, surface saturation boundary, and recharge edge at the times shown in the cross sections are indicated in Figure 5h.

saturation boundary increased linearly by 1.7 s cm^{-1} into the subsurface (Figure 7b). This time lag is a result of downward flow of water infiltrated during each swash event.

Subsurface saturation in the landward reaches of the swash zone experienced the largest fluctuations in response to swash inundation due to the lower frequency of swash events reaching this section of the beach and lower overall levels of saturation near the beach surface (Figure 8). Only the largest swash events were able to reach this region of the swash zone, allowing for greater infiltration into dryer and well-drained sediments compared to farther seaward. The findings are consistent with the pattern of increasing infiltration rates landward in the swash zone observed by Heiss *et al.* [2014].

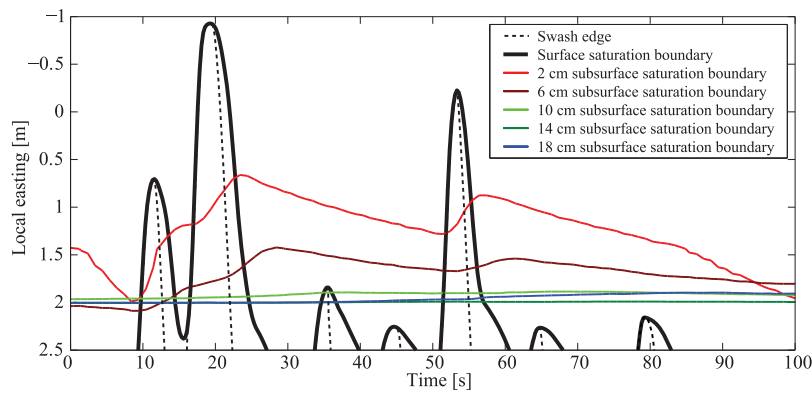


Figure 6. Cross-shore position of the swash edge, surface saturation boundary, and subsurface saturation boundaries at selected depths in the swash zone. Seaward is to the bottom of the figure. Time is relative to 8200 s.

3.1.3. Saturation Dynamics Over a Tidal Cycle

On a tidal time scale, the aquifer sediments near the high tide mark varied from almost fully saturated to unsaturated. The recharge lens appeared immediately following the first swash event that inundated the transect and became more well defined as the swash zone moved landward due to the rising tide (Figures 9a–9c). Swash infiltration and a rising water table eventually saturated the shallow and deeper regions of the initially unsaturated zone, respectively (Figures 9d and 9e). Subsurface saturation reached a maximum 60 min before high tide (Figure 9f) and began to decline between $x = 0$ and 1 m 50 min after high tide (Figure 9g). The offset was caused by swash infiltration, which maintained saturated conditions up to 4 m landward of the tide level. Enough pore water was able to drain from the beach to result in lower subsurface saturation only when the swash zone moved seaward of each measurement location. Subsurface saturation in the landward portion of the swash zone decreased further as the water table and tide level fell (Figure 9h). Once the upper limit of the swash zone was seaward of the transect, the water table fell 0.17 m (Figures 9h–9i). The seaward movement of the swash zone coincided with a further reduction in subsurface saturation throughout the measurement area (Figure 9i). These results demonstrate that the recharge lens was present during flood tide only. The absence of the recharge lens 2 h following high tide was the result of the close proximity of water table and capillary fringe to the sand surface. The water table and capillary fringe maintained saturated conditions below the part of the beach that was periodically inundated and prevented the formation of a recharge lens. As a result, the unsaturated portion of the beachface was

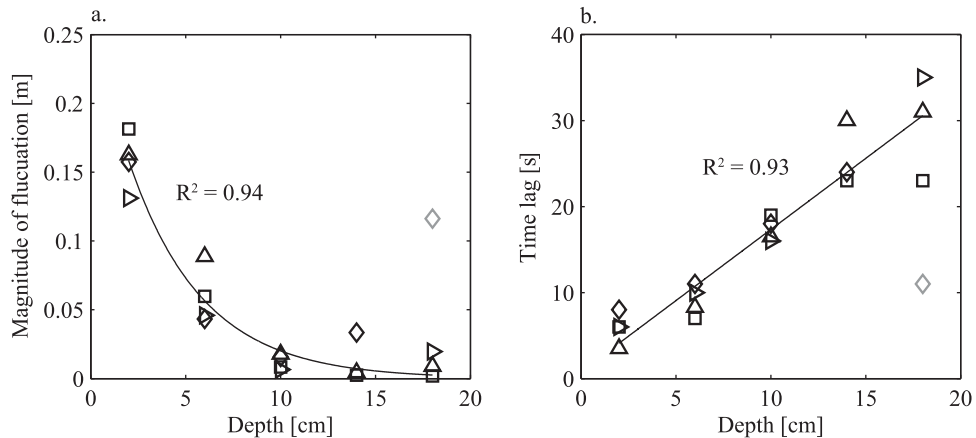


Figure 7. Surface and subsurface saturation boundary response. (a) Magnitude of the fluctuation of the subsurface saturation boundary at various depths normalized to the movement of the surface saturation boundary for each swash event; (b) time lag between the instance of the most landward extent of the subsurface saturation boundary relative to that of the surface saturation boundary as a function of depth. The symbols represent five different swash events that prompted a movement of the subsurface saturation boundary at all depths. The gray symbols represent fluctuations and time lags caused by underlying water table oscillations and were therefore not included in the curve fitting procedure. R^2 is the coefficient of determination of the fitted curves.

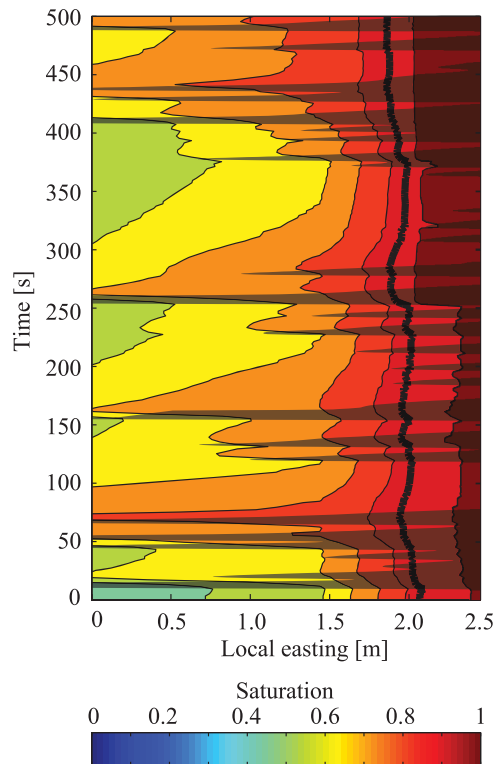


Figure 8. Subsurface saturation across the instrument transect at 2 cm depth. The subsurface saturation boundary (defined as 95% saturation) is shown by the thick black line. The position of the surface saturation boundary is shown by the area shaded black. Seaward is to the right. Time is relative to 8200 s.

lary fringe at 1750 s. Infiltration farther landward at Site C led to higher saturation in the shallow unsaturated zone in comparison to Site B. For instance, saturation greater than 50% at Site C extended to more than twice the depth of that at Site B (14 cm versus 6 cm; Figure 10). Thus, pore space in the shallow unsaturated zone toward the seaward end of the swash zone filled with water due to swash infiltration, while the deeper portion succumbed to a capillary fringe rising together with the water table.

3.3. Infiltration, Recharge, and Discharge Zone Dynamics

The surface saturation boundary and swash edge were coincident during runup and then diverged during rundown as the seaward movement of the surface saturation boundary lagged behind the more rapidly moving swash edge (Figure 11b). This finding is in agreement with previous field studies [e.g., Aagaard and Holm, 1989; Holman *et al.*, 1993; Puleo, 2009; Huisman *et al.*, 2011; Vousdoukas, 2014]. The surface saturation boundary was also consistently decoupled from the extrapolated water table-beachface intersection, which was located farther seaward and generally was the seaward limit of the surface saturation boundary (Figure 11b), which means that it was also decoupled from the exit point, confirming other studies demonstrating surface-subsurface flow decoupling [e.g., Austin and Masselink, 2006; Steenhauer *et al.*, 2011]. The exit point was located within the permanently saturated beachface seaward of the surface saturation boundary and was undetectable from the surface. The dynamics of the extrapolated water table-beachface intersection, subsurface saturation, swash location, exit point, and tide level provide insight into the transient nature of the infiltration, recharge, and discharge zones across the beachface at the tidal and swash event time scale.

The zone of infiltration into the unsaturated zone was more extensive on rising tide than on falling tide, whereas the zone of subaerial discharge was larger on falling tide compared to rising tide. The extrapolated water table-beachface intersection and location of the tide on the beachface moved landward at similar rates from 0 to 5000 s and the distance between them, an indication of the maximum width of the subaerial

located farther landward in the swash zone compared to rising tide. Swash infiltration was limited to a few swash events large enough to extend over the wide saturated beachface and onto the unsaturated beachface.

3.2. Mechanisms of Subsurface Saturation

Subsurface saturation occurred due to a combination of swash infiltration and a rising water table and capillary fringe, with the relative importance of each process depending on the position in the swash zone. At the seaward end of the transect at Site B, the initially unsaturated zone became saturated both from the sand surface downward and from the base of the unsaturated zone upward (Figures 10d–10f). Downward saturation was due to swash infiltration whereas upward saturation was the result of a rising capillary fringe (since the water table was observed to be below the deepest moisture sensor). The rise of the capillary fringe coincided with a water table that rose due to swash-derived unsaturated flow from above in addition to lateral tidal inputs. The top of the capillary fringe is visible from 700 to 1600 s in Figure 10e and its thickness (20 cm) was taken as the distance between the water table and the 95% saturation contour directly above. The predicted thickness of 18 cm based on an empirical approximation [Turner and Nielsen, 1997] and the field site grain size (0.39 mm) agrees well with the observed thickness. The unsaturated zone decreased in thickness until infiltrating water merged with the capillary

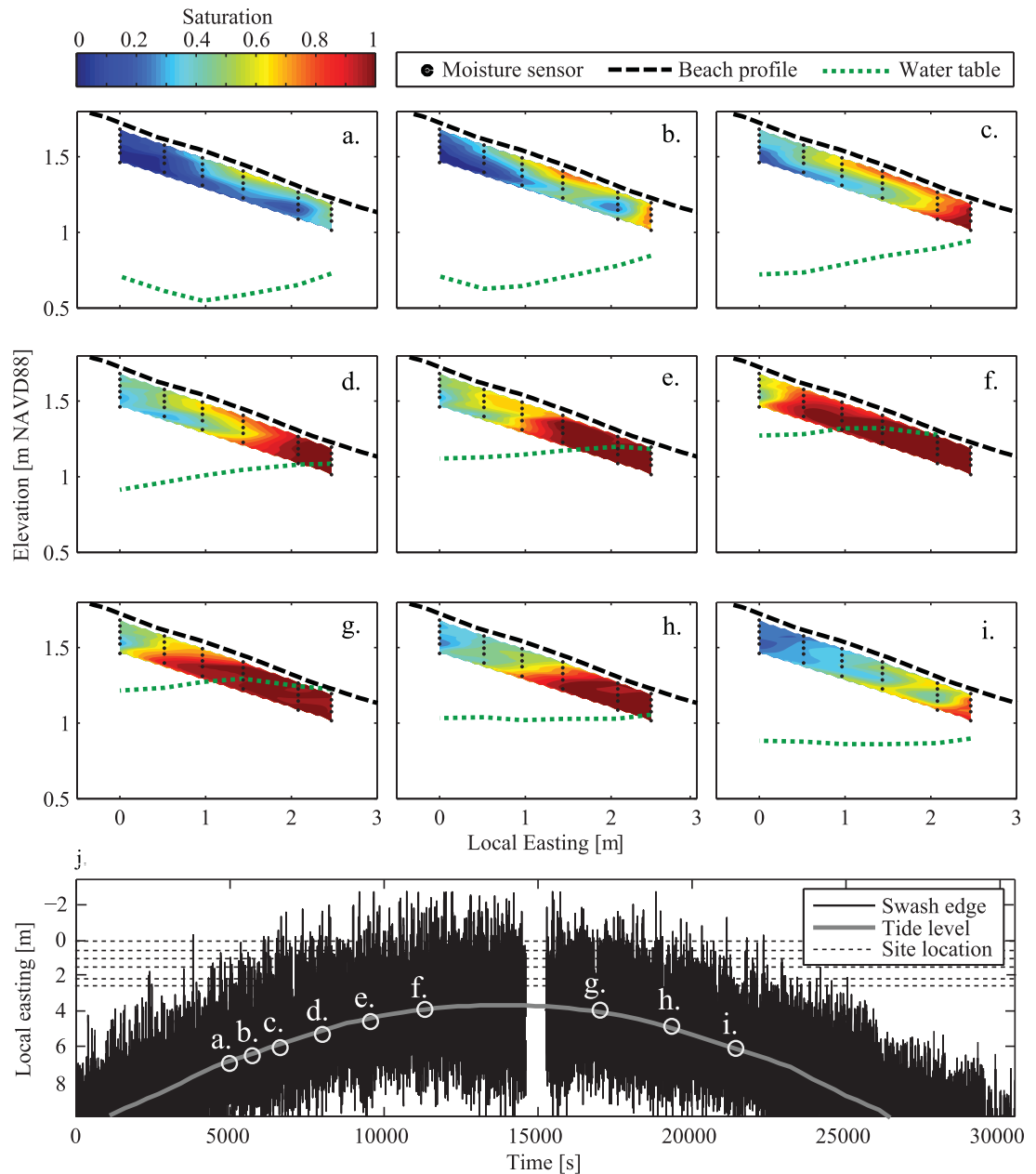


Figure 9. Subsurface saturation and water table elevation averaged over 15 min intervals over the tidal cycle. The position of the tide level on the beachface at the times represented in the cross sections is indicated by the labels in Figure 9j.

discharge zone, remained roughly constant at 0.5 m (Figure 11a). The maximum width of the subaerial discharge zone increased to 1.5 m near high tide at 5000 s when the rate of rising tide began to slow and then doubled to 3 m during ebb tide as the rate of tidal fall outpaced the seaward movement of the extrapolated water table-beachface intersection (Figure 11a). Consequently, the infiltration zone was narrower during ebb tide—the maximum extent of the subaerial discharge zone occupied a larger portion of the swash zone. The opposite occurred during rising tide where the maximum extent of the subaerial discharge zone was narrow and hence infiltration was more widespread.

The width of the infiltration zone at the swash time scale was most variable, followed by the recharge zone, the subaerial discharge zone, and the submarine discharge zone. The width of the infiltration zone varied up to 7 m between swashes as it transited the intermittently saturated beachface with the swash edge. In contrast, the width of the recharge zone was less variable and shifted on the order of 0.5–1.0 m when the

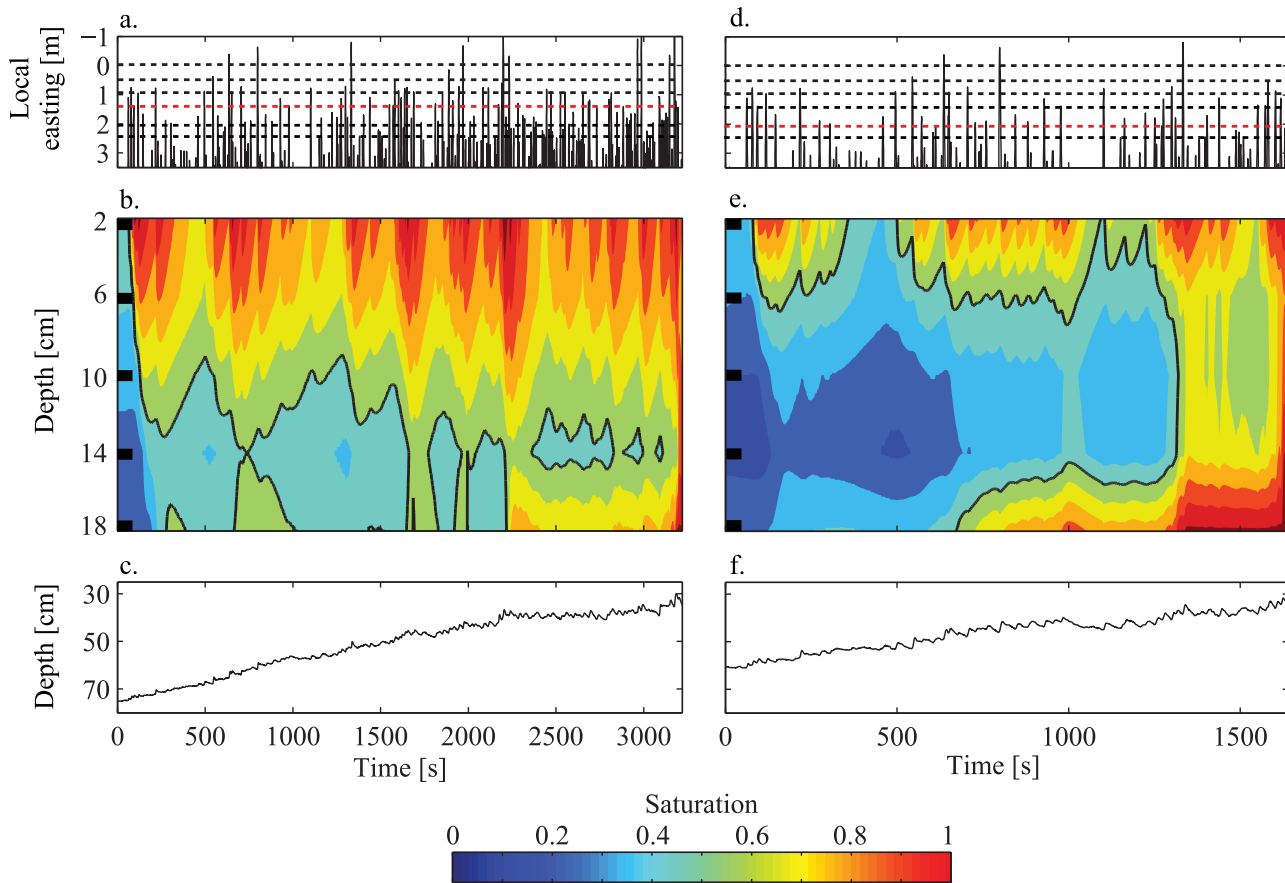


Figure 10. Vertical 1-D subsurface saturation profiles as a function of time at (left) Site C and (right) Site B. (a) Swash edge position, (b) subsurface saturation, and (c) water table depth at Site C. (d) Swash edge position, (e) subsurface saturation, and (f) water table depth at Site B. The dashed horizontal lines are the cross-shore positions of the instrument sites. The red dashed horizontal line is the position of (left) Site C and (right) Site B. The time frame in the right plots is of the first 1500 s of the time shown in the left plots, because the array at Site B becomes fully saturated at 1800 s. The black filled rectangles on the y axis show the depth of the moisture sensors. The black contours in Figures 10b and 10e are 50% saturation. Time is relative to 6020 s.

swash edge came to within a meter of the recharge edge (Figure 11b). The recharge edge was located in the farthest landward section of the swash zone, typically 0.5–1.5 m landward of the runup limit of the largest swash events (Figure 11b). The spatial offset between the recharge edge and the nearby runup limits suggests that landward flow occurs in the unsaturated zone in response to swash, consistent with the landward transport of microspheres in swash zone sediments observed by *Gast et al. [2015]*. The extrapolated water table-beachface intersection, marking the maximum landward extent of the subaerial discharge zone, moved on the order of several centimeters between individual swash events (Figure 11b). The exit point was within the transect for approximately 1.3 h near high tide and also moved on the order of several centimeters between swashes during that period (Figure 11a). Farther seaward, the landward extent of the submarine discharge zone was unchanged as shown by the tide level over the 475 s time period (Figure 11b). The results demonstrate that the width and location of the subaerial discharge zone were controlled primarily by the tide, and the width of the infiltration zone was controlled primarily by swash, while its location varied in response to both swash and the tide.

3.4. Cross-Shore Saturated and Unsaturated Infiltration Rates

The lysimeter collected infiltrating water driven by swash into the saturated portion of the beach within the capillary fringe. The moisture sensors confirmed that flow into the lysimeter did not occur until sediment surrounding the lysimeter was nearly or fully saturated. The time when the perched water table formed and collection began is shown in the beginning of the time series in Figure 12. Water depth inside the lysimeter increased with each swash event that inundated Site A (Figure 12b) and remained steady between events, forming the staircase pattern in Figure 12a. Infiltration ranged

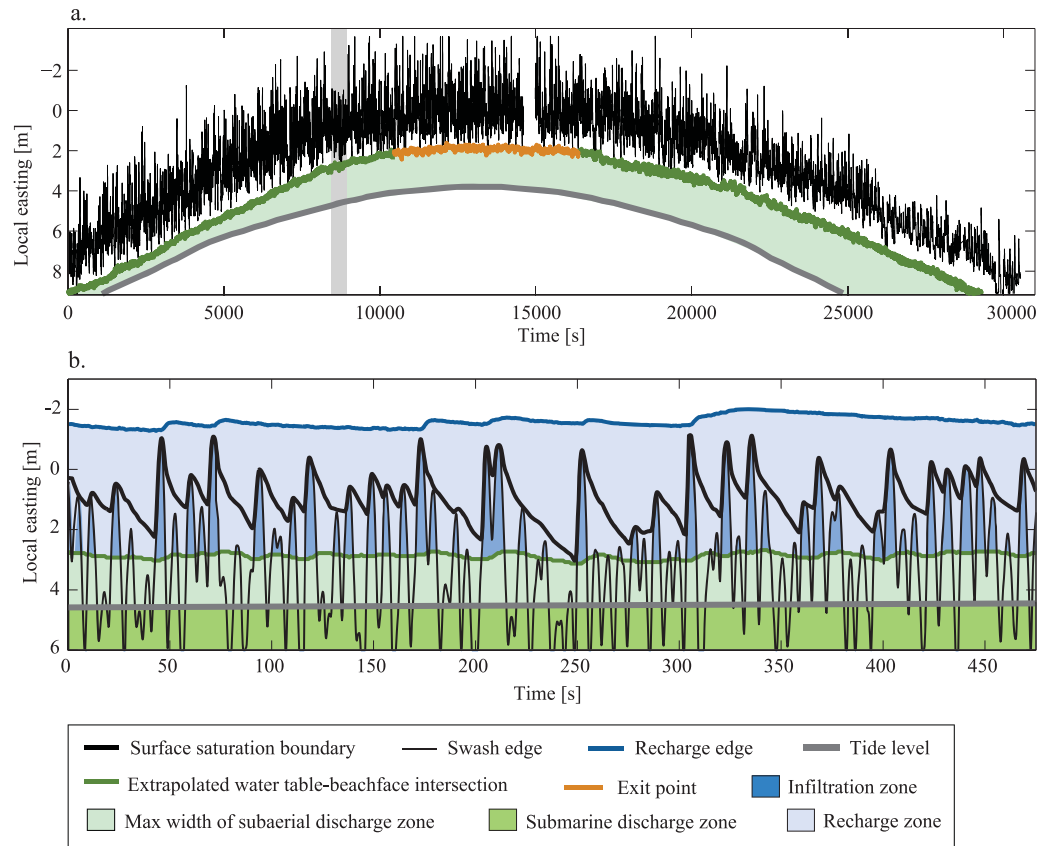


Figure 11. Infiltration, recharge, and discharge zones at the tidal and swash time scale. (a) Surface saturation boundary, exit point, extrapolated water table-beachface intersection, tide level, and maximum width of the subaerial discharge zone on the beachface over the 8.5 h data collection period; (b) inset of shaded gray region in top plot over an 8 min time interval with infiltration, recharge, subaerial discharge, and submarine discharge zones indicated. Seaward is to the bottom in both plots.

from 2 to 14 mm per swash event with greater infiltration generally occurring under longer duration swash events. The 2–14 mm infiltration range translates to a water table fluctuation of 7–47 mm assuming a porosity of 0.3 [e.g., Heiss *et al.*, 2014] and agrees well with the observed 10–50 mm water table fluctuations over this time period, supporting the utility of lysimeters for measuring infiltration in the swash zone.

The lysimeter measurements of infiltration across the saturated beach and calculated infiltration based on saturation across the landward unsaturated beach provide an infiltration profile across the full swash zone. Infiltration per swash event increased in the landward direction from the saturated to unsaturated swash zone. Six swash events extended up to or beyond Site C between 200 and 400 s (Figures 12a and 12b), and unsaturated infiltration was calculated for each event using equation (1). Unsaturated infiltration at Sites A and B could not be determined because the capillary fringe was in contact with the beach surface and hence there was no change in saturation. Estimated infiltration across the unsaturated beachface was lowest at Site C and increased to Site F (Table 1). Comparison between infiltration rates based on the lysimeter and saturation shows that flow across the saturated portion of the swash zone was less than that across the unsaturated beachface. Average infiltration per swash was 8.1 mm across the saturated beach at Site A and 10.9 mm across the unsaturated beachface between Sites C and F. Infiltration was less across the saturated beach, likely due to the presence of the capillary fringe at the sand surface at the location of the lysimeter, which limited infiltration relative to the unsaturated swash zone. Although average infiltration per swash event increased landward from the saturated to unsaturated beachface, total infiltration over the 200 s time span did not increase monotonically landward because all six swash events did not reach the most landward sites. Thus, total inflow increased from Sites A to D before decreasing from Sites D to F.

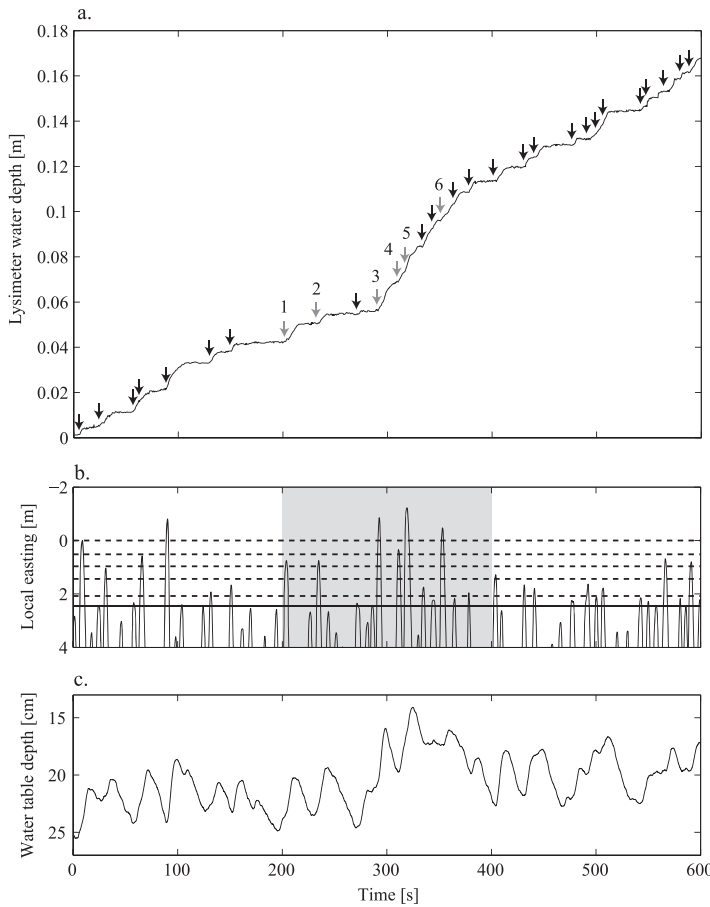


Figure 12. Lysimeter measurements and surrounding conditions. (a) Water depth in the lysimeter at Site A. Black arrows indicate when Site A was inundated by swash. The gray arrows indicate the swash events where infiltration was calculated from moisture response, only events that inundated the beachface landward of Site A were used; (b) cross-shore position of the swash edge. The gray shading is the time interval where infiltration was calculated using equation (1). The dashed horizontal lines are the cross-shore positions of the instrument sites. The solid horizontal line is the position of Site A; (c) water table relative to the sand surface. Time is relative to 7900 s.

4. Discussion

4.1. Subsurface Observations Reveal Infiltration and Discharge Zones

The combined surface and subsurface measurements reveal previously unobserved groundwater-surface water interactions in the swash zone. Previous studies have used the surface saturation boundary as a proxy for the exit point on fine to very coarse grained beaches [e.g., Aagaard and Holm, 1989; Holman *et al.*, 1993; Cartwright *et al.*, 2006; Puleo, 2009; Huisman *et al.*, 2011; Voudoukas, 2014]. The results of this study suggest that the surface saturation boundary and exit point are distinct features on the beach that are consistently decoupled at swash and tidal time scales.

Subsurface saturation in the swash zone is affected by both infiltration and discharge processes. Infiltration occurs on the landward region of the beach beneath the part of the swash that overrides the exit point. The presence of

Table 1. Calculated Infiltration (mm) Per Swash Event From Lysimeter (Site A) and Saturation (D_{sw}) Sites C–F) Measurements^a

	Swash 1	Swash 2	Swash 3	Swash 4	Swash 5	Swash 6	Total	Average
Site A	7.6	4.6	12.7	4.8	11.5	7.4	48.6	8.1
Site C	8.5	5.1	13.6	5.3	12.5	7.8	52.8	8.8
Site D	9.1	5.5	14.9	5.8	13.5	8.4	57.2	9.5
Site E			16.1	6.0	14.2	9.0	45.3	11.3
Site F			16.9		15.2	9.9	42.0	14.0

^aSwash # corresponds to the labels in Figure 12a.

a zone of infiltration across a portion of the saturated beachface contradicts the notion that the entirety of the saturated beachface seaward of the surface saturation boundary is a zone of groundwater discharge and verifies the laboratory findings of Steenhauer *et al.* [2011]. Thus, use of the surface saturation boundary to identify the location of the subaerial discharge zone may lead to an incorrect and large offset relative to its true location. The occurrence and magnitude of the offset will vary with beach slope, hydraulic conductivity, wave conditions, and width of the intertidal zone. The present results demonstrate that identifying the infiltration and subaerial discharge zones can be achieved only through coupled surface and subsurface measurements.

The decoupling between the surface saturation boundary and exit point has important implications for the dynamics of the infiltration, recharge, and discharge zones. Previous studies have used water table measurements to demonstrate that the exit point closely tracks tide level during rising tide, but becomes decoupled during ebb tide [e.g., Turner, 1993; Turner and Masselink, 1998]. Our results confirm these observations and further show that the location and maximum width of the subaerial discharge zone is controlled primarily by the tide rather than individual swash events, even in the moderate wave-energy environment at Herring Point. The swash edge moved across a larger portion of the beachface compared to the extrapolated water table-beachface intersection, suggesting that the infiltration zone is more dynamic than the subaerial discharge zone. However, the recharge zone occupied an area that was more consistent in size than the dynamic infiltration zone. Observations on both rising and falling tides further indicate an asymmetry in infiltration and discharge. On rising tide, the size of the zone of infiltration is large relative to the maximum width of the subaerial discharge zone, whereas on falling tide, the infiltration zone is smaller.

4.2. Implications for Biogeochemistry and Sediment Transport

Beach aquifers host a range of biogeochemical processes that affect the fluxes of dissolved materials from the coast to the ocean through SGD [Moore, 1999; Charette and Sholkovitz, 2006; Hays and Ullman, 2007; Santos *et al.*, 2008; Santoro, 2010]. The maintenance of biogeochemical reactivity within the aquifer is in part dependent on the supply of labile organic carbon and oxygen that enters the beach through wave, tidal, and swash-driven processes. The location and nature of the addition of these seawater-derived constituents into the beach aquifer will affect their transport, degradation, and mixing with through-flowing freshened groundwater. This study demonstrates that infiltration occurs under both saturated and unsaturated conditions in the beachface, but is dynamic in both space and time. Much of the infiltration of water and associated solutes and particles occurs in the intermittently saturated zone in the upper part of the swash zone. However, the transport of reactive solutes and particles from their entry point in the infiltration zone to zones of reactivity in the subsurface ultimately relies on the dynamics of the groundwater flow system which can change over swash [e.g., Turner and Masselink, 1998; Sous *et al.*, 2013; Heiss *et al.*, 2014] and tidal cycles [e.g., Riedel *et al.*, 2010; Befus *et al.*, 2013; Heiss and Michael, 2014]. Because flow within the beach depends on hydraulic gradients and moisture conditions and thus on the location of the infiltration zone, which varies though the tidal cycle, the fate of reactive constituents will likely also differ with their entry point as the swash and infiltration zones move with the tide.

The relative size and location of the infiltration and discharge zones may also influence the stability of the beach. The present results show that a region of the saturated beachface is an area of infiltration, implying a smaller subaerial discharge zone relative to what would be expected based on the full width of the saturated beachface. Infiltration and discharge play important roles in controlling the thickness of the boundary layer and bed shear stress, as well as impacting the effective weight of the sediment [Nielsen, 1992; Turner and Masselink, 1998; Masselink and Li, 2001; Bakhtyar *et al.*, 2011], with the relative importance of boundary layer effects and effective sediment weight dependent on a critical grain size [e.g., Butt *et al.*, 2001; Karambas, 2003]. Thus, the modified size of infiltration and discharge zones relative to previous conceptual understanding that is based on beachface saturation is likely to be important for cross-shore sediment transport as boundary layer effects and the influence of effective sediment weight are adjusted accordingly. Moreover, additional loss of water from the swash lens to the subsurface during runup in comparison to that which would occur over a discharge zone could enhance differences in velocity and flow duration between runup and rundown, potentially altering cross-shore sediment transport.

5. Conclusions

High-frequency surface and subsurface measurements in the swash zone together with simultaneous measurements of saturation and water table elevation within the beach and the position of the swash edge and

surface saturation boundary on the beachface provide new insights into the coupled behavior of swash processes, tides, infiltration, and aquifer recharge and discharge in the intertidal zone.

A region of elevated saturation is formed in the shallow unsaturated zone due to swash infiltration across the unsaturated beachface. This recharge lens indicates vertical unsaturated flow to the water table. The landward extent of the lens responds to swash, but its motion is muted relative to the rapidly moving swash edge, indicating that downward flow in the unsaturated zone and recharge to the aquifer continues after runup. The recharge lens is present only during flood tide because few swash events are capable of overriding a widening subaerial discharge zone during ebb tide.

The initially unsaturated zone becomes saturated due to a combination of vertical infiltration from above and a rising water table and capillary fringe from below, with the relative importance varying with location on the beach. Vertical infiltration is the dominant subsurface saturation mechanism in the landward swash zone, while a rising water table and capillary fringe is more significant farther seaward.

The results of this study show that the location of the surface saturation boundary does not necessarily correspond to the location of the exit point. At Herring Point, the exit point is located farther seaward than the surface saturation boundary. Infiltration occurs landward of the exit point beneath the swash edge, and groundwater discharge occurs seaward of the exit point to the tide level. These results further indicate that surface observations alone cannot be used to correctly identify the location of the intersection of the water table with the beachface or to delineate zones of beachface infiltration and discharge.

The results show for the first time the dynamics of zones of infiltration, recharge, and discharge at the swash and tidal time scale. The infiltration zone and the maximum width of the subaerial discharge zone varied with the tide, though asymmetrically: the infiltration zone was more extensive during flood tide than ebb tide and the maximum width of the subaerial discharge zone was greater during ebb tide. On a swash event time scale, the surface saturation boundary moved across the beach independently of the location of infiltration and subaerial discharge. The zone of infiltration moved together with the swash edge and was the most dynamic region on the beachface. The findings demonstrate that the maximum width of the subaerial discharge zone was controlled primarily by the tide and the infiltration zone was controlled by swash.

Lysimeter measurements beneath the saturated beach and saturation profiles in the unsaturated beach provide, for the first time, insights into the spatial distribution of infiltration across the full swash zone at the time scale of individual swash events. Average infiltration per swash event is greater across the upper unsaturated beachface in comparison to the lower saturated beachface. However, total infiltration across the upper half of the swash zone is smaller due to infrequent swash inundation across that section of the beach.

Groundwater-surface water interactions in the swash zone at swash and tidal time scales are complex and need to be considered when identifying zones of infiltration and discharge on sandy beaches. The subsurface saturation dynamics and time scales of flow in the unsaturated zone have potentially important implications for the biogeochemistry of beach aquifers and for the modeling of sediment transport processes in the swash zone. Models that incorporate beachface saturation as a proxy for infiltration and groundwater discharge will need to be reexamined to more accurately characterize the distribution of vertical flow across the sand surface.

References

- Aagaard, T., and J. Holm (1989), Digitization of wave run-up using video records, *J. Coastal Res.*, 5(3), 547–551.
- Anwar, N., C. Robinson, and D. A. Barry (2014), Influence of tides and waves on the fate of nutrients in a nearshore aquifer: Numerical simulations, *Adv. Water Resour.*, 73, 203–213, doi:10.1016/j.advwatres.2014.08.015.
- Austin, M. J., and G. Masselink (2006), Swash–groundwater interaction on a steep gravel beach, *Cont. Shelf Res.*, 20, 2503–2519.
- Bakhtyar, R., A. Brovelli, D. A. Barry, and L. Li (2011), Wave-induced water table fluctuations, sediment transport and beach profile change: Modeling and comparison with large-scale laboratory experiments, *Coastal Eng.*, 58(1), 103–118, doi:10.1016/j.coastaleng.2010.08.004.
- Baldock, T. E., A. J. Baird, D. P. Horn, and T. Mason (2001), Measurements and modelling of swash-induced pressure gradients in the surface layers of a sand beach, *J. Geophys. Res.*, 106(C2), 2653–2666.
- Befus, K. M., M. B. Cardenas, D. V. Erler, I. R. Santos, and B. D. Eyre (2013), Heat transport dynamics at a sandy intertidal zone, *Water Resour. Res.*, 49, 3770–3786, doi:10.1002/wrcr.20325.
- Bews, B. E., S. L. Barbour, G. W. Wilson, and M. A. O’Kane (1997), The design of lysimeters for a low flux cover system over acid generating waste rock, paper presented at the 50th Canadian Geotechnical Conference, the Can. Geotech. Soc., Ottawa.
- Boufadel, M. C., H. Li, M. T. Suidan, and A. D. Venosa (2007), Tracer studies in a laboratory beach subjected to waves, *J. Environ. Eng.*, 133, 722–732, doi:10.1061/(ASCE)0733-9372(2007)133:7(722).

Acknowledgments

The authors thank University of Delaware faculty and students Thomas McKenna, Aline Pieterse, Thijss Lanckriet, Adam Dejean, Veronica Citerone, Hannah Billian, Jillian McKenna, Nathan Veale, and Christopher Russoniello for assistance in the field. Zachary Nerwinski is acknowledged for his assistance with runup and surface saturation boundary digitization. This research was supported by National Science Foundation (NSF) grants EAR-1246554 (to H.M. and W.J.U.), EAR-0910756 (to H.M.), and OCE-1332703 (to J.A.P.), and by Delaware EPSCoR with funds from NSF EPS-0814251 and the State of Delaware (to H.M. and W.J.U.). The data used to produce the results of this paper may be obtained from the corresponding author.

- Butt, T., P. Russell, and I. Turner (2001), The influence of swash infiltration–exfiltration on beach face sediment transport: Onshore or offshore?, *Coastal Eng.*, 42, 35–52.
- Cartwright, N., T. E. Baldock, P. Nielsen, D.-S. Jeng, and L. Tao (2006), Swash-aquifer interaction in the vicinity of the water table exit point on a sandy beach, *J. Geophys. Res.*, 111, C09035, doi:10.1029/2005JC003149.
- Charbonnier, C., P. Anschutz, D. Poirier, S. Bujan, and P. Leroart (2013), Aerobic respiration in a high-energy sandy beach, *Mar. Chem.*, 155, 10–21, doi:10.1016/j.marchem.2013.05.003.
- Charette, M. A., and E. R. Sholkovitz (2002), Oxidative precipitation of groundwater-derived ferrous iron in the subterranean estuary of a coastal bay, *Geophys. Res. Lett.*, 29(10), 1444, doi:10.1029/2001GL014512.
- Charette, M. A., and E. R. Sholkovitz (2006), Trace element cycling in a subterranean estuary: Part 2. Geochemistry of the pore water, *Geochim. Cosmochim. Acta*, 70(4), 811–826, doi:10.1016/j.gca.2005.10.019.
- Gast, R. J., S. Elgar, and B. Raubenheimer (2015), Observations of transport of bacterial-like microspheres through beach sand, *Cont. Shelf Res.*, 97, 1–6, doi:10.1016/j.csr.2015.01.010.
- Geng, X., and M. C. Boufadel (2015), Numerical study of solute transport in shallow beach aquifers subjected to waves and tides, *J. Geophys. Res. Oceans*, 120, 1409–1428, doi:10.1002/2014JC010539.
- Hays, R. L., and W. J. Ullman (2007), Direct determination of total and fresh groundwater discharge and nutrient loads from a sandy beach-face at low tide (Cape Henlopen, Delaware), *Limnol. Oceanogr.*, 52(1), 240–247, doi:10.4319/lo.2007.52.1.00240.
- Hegge, B. J., and G. Masselink (1991), Groundwater-table responses to wave run-up: An experimental study from Western Australia, *J. Coastal Res.*, 7(3), 623–634.
- Heiss, J. W., and H. A. Michael (2014), Saltwater-freshwater mixing dynamics in a sandy beach aquifer over tidal, spring-neap, and seasonal cycles, *Water Resour. Res.*, 50, 6747–6766, doi:10.1002/2014WR015574.
- Heiss, J. W., W. J. Ullman, and H. A. Michael (2014), Swash zone moisture dynamics and unsaturated infiltration in two sandy beach aquifers, *Estuarine Coastal Shelf Sci.*, 143, 20–31, doi:10.1016/j.ecss.2014.03.015.
- Holland, K. T., and R. A. Holman (1993), The statistical distribution of swash maxima on natural beaches, *J. Geophys. Res.*, 98(C6), 10,271–10,278.
- Holland, K. T., R. A. Holman, T. C. Lippmann, J. Stanley, and N. Plant (1997), Practical use of video imagery in nearshore oceanographic field studies, *J. Oceanic Eng.*, 22(1), 81–92.
- Holman, R. A., A. H. Sallenger Jr., T. C. Lippmann, and J. W. Haines (1993), The application of video image processing to the study of near-shore processes, *Oceanography*, 6(3), 78–85.
- Hoque, Md., and T. Asano (2007), Numerical study on wave-induced filtration flow across the beach face and its effects on swash zone sediment transport, *Ocean Eng.*, 34, 2033–2044.
- Horn, D. P., T. E. Baldock, A. J. Baird, and T. E. Mason (1998), Field measurements of swash induced pressures within a sandy beach, paper presented at 26th International Conference on Coastal Engineering, American Society of Civil Engineers, Copenhagen, Denmark.
- Huisman, C. E., K. R. Bryan, G. Coco, and B. G. Ruessink (2011), The use of video imagery to analyse groundwater and shoreline dynamics on a dissipative beach, *Cont. Shelf Res.*, 31(16), 1728–1738, doi:10.1016/j.csr.2011.07.013.
- Jemison, J. M., and R. H. Fox (1992), Estimation of zero-tension pan lysimeters collection efficiency, *Soil Sci.*, 15, 85–94.
- Jordan, C. F. (1968), A simple, tension-free lysimeter, *Soil Sci.*, 105, 81–86.
- Kang, H.-Y., P. Nielsen, and D. J. Hanslow (1994), Watertable overheight due to wave runup on a sandy beach, paper presented at the 24th International Conference of Coastal Engineering, American Society of Civil Engineers, Kobe, Japan.
- Karambas, T. V. (2003), Modelling of infiltration-exfiltration effects of cross-shore sediment transport in the swash zone, *Coastal Eng.*, 45(1), 63–82, doi:10.1142/S057856340300066X.
- Kroeger, K. D., and M. A. Charette (2008), Nitrogen biogeochemistry of submarine groundwater discharge, *Limnol. Oceanogr.*, 53(3), 1025–1039, doi:10.4319/lo.2008.53.3.1025.
- Li, L., D. A. Barry, and C. B. Pattiaratchi (1997), Numerical modelling of tide-induced beach water table fluctuations, *Coastal Eng.*, 30(1-2), 105–123, doi:10.1016/S0378-3839(96)00038-5.
- Li, L., D. A. Barry, F. Stagnitti, and J. Y. Parlange (1999), Submarine groundwater discharge and associated chemical input to the coastal sea, *Water Resour. Res.*, 35(11), 3253–3259.
- Masselink, G., and L. Li (2001), The role of swash infiltration in determining the beachface gradient: A numerical study, *Mar. Geol.*, 176, 139–156.
- Masselink, G., and I. L. Turner (2012), Large-scale laboratory investigation into the effect of varying back-barrier lagoon water levels on gravel beach morphology and swash zone sediment transport, *Coastal Eng.*, 63, 23–38, doi:10.1016/j.coastaleng.2011.12.007.
- McAllister, S. M., J. M. Barnett, J. W. Heiss, A. J. Findlay, D. J. Macdonald, C. L. Dow, G. W. Luther III, H. A. Michael, and C. S. Chan (2015), Dynamic hydrologic and biogeochemical processes drive microbially enhanced iron and sulfur cycling within the intertidal mixing zone of a beach aquifer, *Limnol. Oceanogr.*, 60, 329–345, doi:10.1002/lno.10029.
- McLachlan, A., I. G. Eliot, and D. J. Clarke (1985), Water filtration through reflective microtidal beaches and shallow sublittoral sands and its implications for an inshore ecosystem in Western Australia, *Estuarine Coastal Shelf Sci.*, 21, 91–104.
- Michael, H. A., M. A. Charette, and C. F. Harvey (2011), Patterns and variability of groundwater flow and radium activity at the coast: A case study from Waquoit Bay, Massachusetts, *Mar. Chem.*, 127(1-4), 100–114, doi:10.1016/j.marchem.2011.08.001.
- Moore, W. S. (1999), The subterranean estuary: A reaction zone of ground water and sea water, *Mar. Chem.*, 65, 111–125.
- Nielsen, P. (1992), *Coastal Bottom Boundary Layers and Sediment Transport*, Adv. Ser. Ocean Eng., vol. 4, World Sci., Singapore.
- Orr, M., M. Zimmer, D. E. Jelinski, and M. Mews (2005), Wrack deposition on different beach types: Spatial and temporal variation in the pattern of subsidy, *Ecology*, 86(6), 1496–1507.
- Packwood, A. R., and D. H. Peregrine (1980), The propagation of solitary waves and bores over a porous bed, *Coastal Eng.*, 3, 221–242.
- Peters, A., and W. Durner (2009), Large zero-tension plate lysimeters for soil water and solute collection in undisturbed soils, *Hydrolog. Earth Syst. Sci.*, 6(3), 4637–4669, doi:10.5194/hessd-6-4637-2009.
- Puleo, J. A. (2009), Tidal variability of swash-zone sediment suspension and transport, *J. Coastal Res.*, 254, 937–948, doi:10.2112/08-1031.1.
- Riedel, T., K. Lettmann, M. Beck, and H.-J. Brumsack (2010), Tidal variations in groundwater storage and associated discharge from an intertidal coastal aquifer, *J. Geophys. Res.*, 115, C04013, doi:10.1029/2009JC005544.
- Rosenberry, D. O., R. W. Sheibley, S. E. Cox, F. W. Simonds, and D. L. Naftz (2013), Temporal variability of exchange between groundwater and surface water based on high-frequency direct measurements of seepage at the sediment-water interface, *Water Res. Resour.*, 49, 2975–2986, doi:10.1002/wrcr.20198.
- Roy, M., J. B. Martin, J. Cherrier, J. E. Cable, and C. G. Smith (2010), Influence of sea level rise on iron diagenesis in an east Florida subterranean estuary, *Geochim. Cosmochim. Acta*, 74(19), 5560–5573, doi:10.1016/j.gca.2010.07.007.
- Russell, A. E., and J. J. Ewel (1985), Leaching from a tropical andept during big storms: A comparison of three methods, *Soil Sci.*, 139, 181–189.

- Santoro, A. (2010), Microbial nitrogen cycling at the saltwater-freshwater interface, *Hydrogeol. J.*, 18, 187–202, doi:10.1007/s10040-009-0526-z.
- Santos, I. R., W. C. Burnett, J. Chanton, B. M. Mwashote, I. G. N. A. Suryaputra, and T. Dittmar (2008), Nutrient biogeochemistry in a Gulf of Mexico subterranean estuary and groundwater-derived fluxes to the coastal ocean, *Limnol. Oceanogr.*, 53(2), 705–718, doi:10.4319/lo.2008.53.2.0705.
- Sawyer, A. H., O. Lazareva, K. D. Kroeger, K. Crespo, C. S. Chan, T. Stieglitz, and H. A. Michael (2014), Stratigraphic controls on fluid and solute fluxes across the sediment-water interface of an estuary, *Limnol. Oceanogr.*, 59(3), 997–1010, doi:10.4319/lo.2014.59.3.0997.
- Sous, D., A. Lambert, V. Rey, and H. Michallet (2013), Swash–groundwater dynamics in a sandy beach laboratory experiment, *Coastal Eng.*, 80, 122–136, doi:10.1016/j.coastaleng.2013.05.006.
- Spiteri, C., C. P. Slomp, M. A. Charette, K. Tuncay, and C. Meile (2008), Flow and nutrient dynamics in a subterranean estuary (Waquoit Bay, MA, USA): Field data and reactive transport modeling, *Geochim. Cosmochim. Acta*, 72, 3398–3412.
- Steenhauer, K., D. Pokrajac, T. O'Donoghue, and G. A. Kikkert (2011), Subsurface processes generated by bore-driven swash on coarse-grained beaches, *J. Geophys. Res.*, 116, C04013, doi:10.1029/2010JC006789.
- Steenhauer, K., D. Pokrajac, and T. O'Donoghue (2012), Numerical model of swash motion and air entrapment within coarse-grained beaches, *Coastal Eng.*, 64, 113–126, doi:10.1016/j.coastaleng.2012.01.004.
- Talbot, C. A., and F. L. Ogden (2008), A method for computing infiltration and redistribution in a discretized moisture content domain, *Water Resour. Res.*, 44, W08453, doi:10.1029/2008WR006815.
- Thompson, M. L., and R. L. Scharf (1994), An improved zero-tension lysimeter to monitor colloid transport in soils, 24, 378–383.
- Turner, I. L. (1993), Water table outcropping on macro-tidal beaches: A simulation model, *Mar. Geol.*, 115, 227–238.
- Turner, I. L., and G. Masselink (1998), Swash infiltration-exfiltration and sediment transport, *J. Geophys. Res.*, 103(C13), 30,813–30,824.
- Turner, I. L., and G. Masselink (2012), Coastal gravel barrier hydrology—Observations from a prototype-scale laboratory experiment (BAR-DEX), *Coastal Eng.*, 63, 13–22, doi:10.1016/j.coastaleng.2011.12.008.
- Turner, I. L., and P. Nielsen (1997), Rapid watertable fluctuations within the beachface: Implications for swash zone sediment mobility?, *Coastal Eng.*, 32, 45–59.
- Ullman, W. J., B. Chang, D. C. Miller, and J. A. Madsen (2003), Groundwater mixing, nutrient diagenesis, and discharges across a sandy beachface, Cape Henlopen, Delaware (USA), *Estuarine Coastal Shelf Sci.*, 57, 539–52.
- Vousdoukas, M. I. (2014), Observations of wave run-up and groundwater seepage line motions on a reflective-to-intermediate, meso-tidal beach, *Mar. Geol.*, 350, 52–70, doi:10.1016/j.margeo.2014.02.005.
- Waddell, E. (1976), Swash-groundwater-beach profile interactions, in *Beach and Nearshore Sedimentation*, edited by R. A. Davis and R. L. Etherington, *Soc. Econ. Paleontol. Mineral. Spec. Publ.*, 24, 115–125.
- Zhu, Y., R. H. Fox, and J. D. Toth (2002), Leachate collection efficiency of zero-tension pan and passive capillary fiberglass wick lysimeters, *Soil Sci. Soc. Am. J.*, 66, 37–43.